J Nanopart Res (2011) 13:2235–2244
DOI 10.1007/s11051-010-9982-6

RESEARCH PAPER

Magnetic and dielectric properties of $Mn_{0.2}Ni_{0.8}Fe_2O_4$ nanoparticles synthesized by PEG-assisted hydrothermal method

Y. Köseoğlu · M. Bay · M. Tan · A. Baykal · H. Sözeri · R. Topkaya · N. Akdoğan

Received: 7 May 2010 / Accepted: 28 May 2010 / Published online: 18 June 2010

Abstract We present a systematic investigation on the structural and magnetic properties of $Mn_{0.2}Ni_{0.8}Fe_2O_4$ nanoparticles synthesized by a polyethylene glycol (PEG)-assisted hydrothermal route. XRD, FT-IR, TEM and VSM were used for the structural, morphological, dielectric properties and magnetic investigation of the products, respectively. Average crystallite size of product was estimated using Line profile fitting as 6 ± 1 nm and particle size as 6.5 ± 1.0 nm from TEM micrographs. Magnetization measurements have shown that the particles have a blocking temperature of 134 K. Magnetization and the coercive field of the sample increase by decreasing the temperature. The conductivity measurements reveal the semiconducting behaviour for the sample. Temperature-dependent dielectric properties: dielectric permittivity (ε) and ac conductivity (σ_{ac}) for the sample were studied as a function of applied frequency in the range from 1 Hz to 3 MHz. These studies indicated that the dielectric dispersion curve for the sample showed usual dielectric dispersion which can be explained on the basis of Koop's theory, which is based on the Maxwell–Wagner model for the interfacial polarization of homogeneous double structure.

Keywords Hydrothermal synthesis · Coercivity · Magnetic nanomaterials · Spinel ferrites

Y. Köseoğlu (✉) · M. Bay · M. Tan
Department of Physics, Fatih University, Buyukçekmece, 34500 Istanbul, Turkey
e-mail: yukselk@fatih.edu.tr

A. Baykal
Department of Chemistry, Fatih University, Buyukçekmece, 34500 Istanbul, Turkey

H. Sözeri
TUBITAK-UME, National Metrology Institute, PO Box 54, 41470 Gebze, Kocaeli, Turkey

R. Topkaya · N. Akdoğan
Department of Physics, Gebze Institute of Technology, 41400 Gebze, Kocaeli, Turkey

R. Topkaya · N. Akdoğan
Nanomagnetism and Spintronics Research Center (NASAM), Gebze Institute of Technology, 41400 Gebze, Kocaeli, Turkey

Introduction

Nanosized spinel ferrite particles have attracted considerable interest, and efforts continue to investigate them for their technological applications in the microwave industries, disk recording, refrigeration systems, electrical devices, ferrofluids, etc. (McMichael et al. 1992; Ghasemi et al. 2006; Sahoo et al. 2004; Kasapoglu et al. 2007; Ozkaya et al. 2009). The magnetic properties of spinel ferrites can be varied

systematically by changing the identity of the divalent Me^{2+} cations (Me = Co, Mn, Ni, Zn, etc.) without changing the spinel crystal structure (Rondinone et al. 1999).

The spinel structure allows the introduction of different metallic ions, which can change the magnetic and electric properties considerably. For example, due to the antiferromagnetic nature of La^{3+} ions, there is a possibility of achieving control over magnetic parameters like remanence and coercivity in developing technologically important materials by simple substitution of the La^{3+} ions in NiA_xFe_2-xO_4 (Kuznetsov et al. 1999).

Ferrites are well known for their electrical, magnetic and catalytic properties (Shyam et al. 2002; Reddy et al. 2004). The general structure of ferrites with spinel structure is $[M^{2+}]_{tet}$ $[Fe^{3+}]_{octa}O_4$. The introduction of third metal ion modifies the distribution of ions in the spinel structure. Varying the concentration of third metal ion can easily alter distribution of Fe^{3+} ion.

Recent studies have been proved that the substitution of Mn^{3+} reduces the active magnetic linkages, and hence makes T_c decrease with increasing x in $CoFe_{2-x}Mn_xO_4$ system. The decrease in T_c of the present ferrites is very beneficial for the use in magnetic and magneto-optical recording (Zhou et al. 2002; Zhou et al. 2006).

To the best of our knowledge, only the limited number of report is available for the synthesis of $Mn_xNi_{1-x}Fe_2O_4$ nanoparticles (NPs) and bulk by various methods. In this study, we aim to prepare Mn-substituted Ni ferrite NPs with a low sintering temperature involving less energy and low cost metal nitrates as raw materials.

Experimental

Synthesis

0.250 g $MnCl_2$, 1.04 g $NiCl_2$ and 5.4 g of $FeCl_3 \cdot 6H_2O$ were each dissolved in 10 mL distilled water to form a clear solution and mixed. The mixture was stirred with a magnetic stirrer until the reactants were dissolved completely. After that 10 mL PEG (10.000) was added to the solution. And pH of the solution was adjusted to 11.0 by adding 2 M NaOH as dropwise during stirring. After continuous stirring at 400 rpm for an hour, a homogeneous solution could be obtained. The autoclave was kept at 150 °C for 12 h, then was allowed to cool to room temperature. The product was then filtered and washed several times with distilled water and absolute ethanol, and subsequently dried in a vacuum oven at 25 °C for 12 h.

Measurements

X-ray powder diffraction (XRD) analysis was conducted on a Rigaku Smart Lab Diffractometer operated at 40 kV and 35 mA using Cu K_α radiation.

Fourier transform infrared (FT-IR) spectra were recorded in transmission mode with a Perkin Elmer BX FT-IR infrared spectrometer. The powder samples were ground with KBr and compressed into a pellet. FT-IR spectra in the range 4000–400 cm^{-1} were recorded in order to investigate the nature of the chemical bonds formed.

VSM measurements were performed by using a Quantum Design Vibrating sample magnetometer (QD-VSM). The sample was measured between ±10 kOe at room temperature and 10 K. ZFC (zero field cooling) and FC (field cooling) measurements were carried out at 100 Oe and the blocking temperature was determined from the measurements.

Transmission electron microscopy (TEM) analysis was performed using a FEI Tecnai G2 Sphera microscope. A drop of diluted sample in alcohol was dripped on a TEM grid.

The thermal stability was determined by thermogravimetric analysis (TGA, Perkin Elmer Instruments model, STA 6000). The TGA thermograms were recorded for 5 mg of powder sample at a heating rate of 10 °C min in the temperature range of 30–800 °C under nitrogen atmosphere.

Conductivity (ac–dc) measurements of the product were studied by Novocontrol dielectric spectroscopy in the range 20–120 °C with a step of 10 °C (frequency range 0.1 Hz–3 MHz).

Results and discussion

XRD analysis

XRD studies of product confirmed the formation of single phase cubic spinel structure. Typical

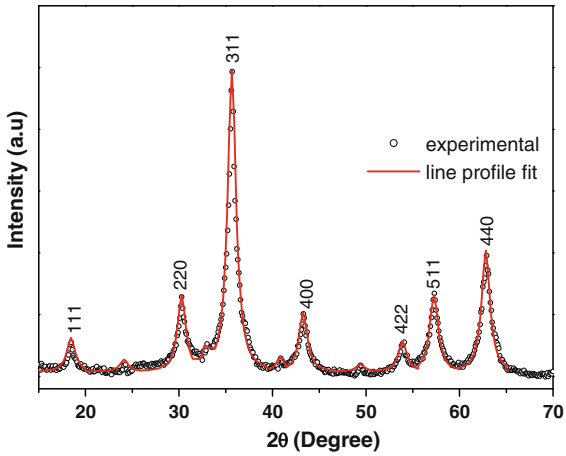

Fig. 1 XRD pattern of $Mn_{0.2}Ni_{0.8}Fe_2O_4$ NP's synthesized by PEG-assisted hydrothermal method

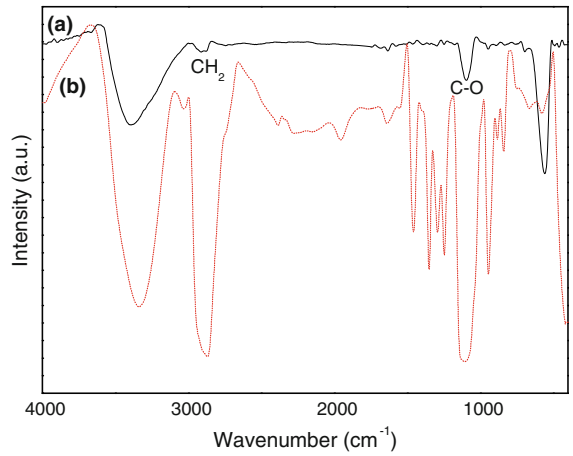

Fig. 2 FTIR spectra of (*a*) $Mn_{0.2}Ni_{0.8}Fe_2O_4$ NP's synthesized by PEG-assisted hydrothermal method (*b*) PEG

microphotograph of $Mn_{0.2}Ni_{0.8}Fe_2O_4$ system is presented in Fig. 1. All of the observed diffraction peaks are indexed by the cubic structure of $NiFe_2O_4$ (JCPDS no. 19-629). The mean size of the crystallites was estimated from the diffraction pattern by line profile fitting method using the equation given in studies of Wejrzanowski et al. (2006) and Pielaszek (2003), as 6 ± 1.0 nm. The line profile, shown in Fig. 1 was fitted for observed eleven peaks with the following miller indices: (111) (220) (311) (400) (422) (511) (440).

FT-IR analysis

Figure 2 shows the IR spectra of as prepared samples at 300 °C. Two mainbroad metal–oxygen bands are seen in the IR spectra of all spinels, and ferrites in particular. The highest one, v_1, (Fig. 2) generally observed in the range 600–550 cm^{-1}, corresponds to intrinsic stretching vibrations of the metal at the tetrahedral site, $M_{tetra} \leftrightarrow O$, whereas the v_2-lowest band, usually observed in the range 450–385 cm^{-1}, is assigned to octahedral-metal stretching, $M_{octa} \leftrightarrow O$ (Sertkol 2008; 2009a, b; Kavas et al. 2009). It is known that Ni^{2+} ions have octahedral-site preference, while Mn^{2+} and Fe^{3+} ions can occupy both octahedral and tetrahedral sites (Liu et al. 2006). The band at 580 and 680 cm^{-1} are the characteristics of NiMn ferrites as reported elsewhere (Liu et al. 2006). However, no clear peak due to octahedrally coordinated metal ions has been observed which is expected to be below 400 cm^{-1}. This may be due to the broadening of this peak attributed to very small particles of spinel ferrites.

The bands observed around 3430 and 1521 cm^{-1} frequencies are ascribed due to the stretching modes and H O H bending vibration of the free or absorbed water molecules.

Thermal analysis

Thermal stability of the precursor powder and final powders has been analyzed using TGA (Fig. 3). To further confirm the existence of PEG on the surface of $Mn_{0.2}Ni_{0.8}Fe_2O_4$ nanoparticles and quantify the proportion of organic and inorganic phase, TGA was

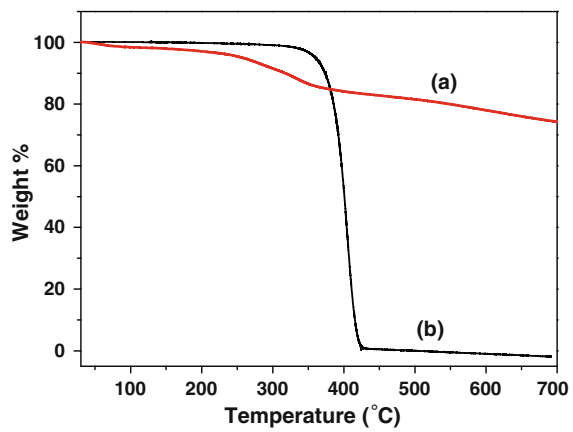

Fig. 3 TGA thermograms of (*a*) $Mn_{0.2}Ni_{0.8}Fe_2O_4$ NP's via PEG-assisted hydrothermal route, and (*b*) PEG

performed in the temperature range of 30–600 °C. Pure PEG combustion started at ~340 °C and completely combusted at ~420 °C (Xiaotun et al. 2003). Evidently, the combustion is delayed for the PEG-coated $Mn_{0.2}Ni_{0.8}Fe_2O_4$ nanoparticles which starts at ~380 °C and completes at ~410 °C. The increase of combustion tempearture is due to the extra interaction between the PEG and $Mn_{0.2}Ni_{0.8}Fe_2O_4$ nanoparticles (Zhang et al. 2008; Li et al. 2007). Up to 400 °C, the observed weight loss for product is due to the adsorbed water. Nanocomposite shows a major weight loss of ~20% over the temperature range of 30–600 °C due to the decomposition and combustion of PEG. This implies that nanocomposite has ~80% inorganic phase as $Mn_{0.2}Ni_{0.8}Fe_2O_4$ nanoparticles.

TEM analysis

TEM micrographs of as-synthesized MnNi ferrite nanoparticles were given in Fig. 4a and their particle size distribution were presented in Fig. 4b. A histogram of the size distribution is fitted to log normal function with 6.5 ± 1.0 nm (by counting 160 nanoparticles) except for some agglomerated particles (which can increase the magnetic interaction between particles, and therefore may influence the magnetic properties of the product).

Magnetic measurements

Figure 5 shows the magnetization loops of the $Mn_{0.2}Ni_{0.8}Fe_2O_4$ nanoparticles at some selected temperatures. As it is seen from the figure, at room temperature, it shows that the sample has no hysteresis. By decreasing the temperature down to 130 K, it also does not show hysteretic behaviour. While the temperature is further decreased, the sample shows hysteretic behaviour vith small coercivity. By decreasing the temperature, the coercivity of the sample is increasing and reaches to a coercivity of 272 Oe at lowest temperature (10 K). The coercivity (H_c) of a magnetic material is generally a measure of its magnetocrystalline anisotropy, but it may also originate from exchange anisotropy due to spin disorder at the particle surface at low temperatures (Sertkol et al. 2010). At all temperatures, the magnetization does not reach the saturation even at 5 kOe applied magnetic field.

Saturation magnetizations (obtained from the linear extrapolation of M vs. 1/H) of 31.48 and 41.96 emu/g are obtained for the room temperature and the lowest temperature measurements. The obtained values of saturation magnetization for $Mn_{0.2}Ni_{0.8}Fe_2O_4$ are much lower than the saturation magnetization of bulk $MnFe_2O_4$ (Ms = 110 emu/g), and of bulk $NiFe_2O_4$ (Ms = 55 emu/g) (Balaji et al. 2002; Smith and Wijn 1959). The absence of saturation, remanent magnetization, and coercivity at high temperature region in the M–H curve indicates the superparamagnetic nature of the particles, which relax back their spins by rotation on removal of applied magnetic field so as to give a zero net magnetic moment. In this case, even though the temperature is below the Curie temperature and the thermal energy is not sufficient to overcome the coupling force between neighboring atoms, the thermal energy is sufficient to change the direction of magnetization of the entire crystallite (Sertkol et al. 2009a, b; Atif et al. 2006). It is also known that fine particles can be easily activated thermally and overcome magnetic anisotropy. Nanoparticles lost their hysteresis property above blocking temperature and magnetic moments follow the same direction with applied magnetic field, so that the magnetic moments do not have any remanent magnetization and a hysteresis loop to observe coercive field. Below the blocking temperature, the particles do not have adequate thermal energy to attain complete thermal equilibrium with the applied field during the measurement time and hence, hysteresis appears. The nonsaturation of the magnetization even at the highest applied field of 5 kOe also implies the presence of single domain nanoparticles in superparamagnetic state (Upadhyay et al. 2007; Chinnasamy et al. 2000).

Figure 6 presents the results of the magnetization measurements of $Mn_{0.2}Ni_{0.8}Fe_2O_4$ nanoparticles obtained in ZFC and FC (with 50 Oe applied field) conditions. The temperature-dependent magnetization of $Mn_{0.2}Ni_{0.8}Fe_2O_4$ nanoparticles increases by decreasing the temperature, and ZFC curve exhibits a relatively broad cusp at around 130 K and achieves maximum at 134 K that corresponds to the blocking temperature, T_B which is a clear signature of superparamagnetism. The broadness in magnetization indicates the existence of particles with different sizes. It can be noted that the FC magnetization also

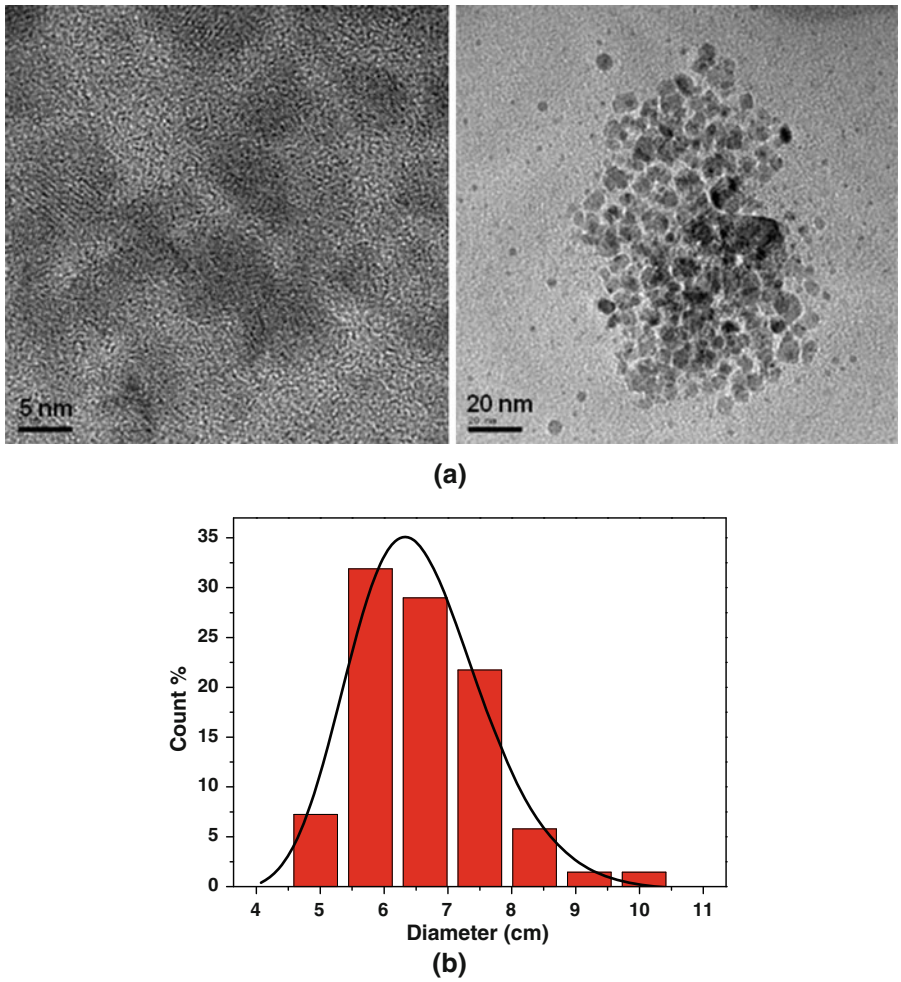

Fig. 4 TEM micrographs (**a**) and calculated histogram (**b**) for as-synthesized $Mn_{0.2}Ni_{0.8}Fe_2O_4$ NP's

increases with decreasing temperature due to clusters ordering along the field direction as seen for field induced cluster glass system.

In magnetic materials, decreasing the size to nanometer dimensions leads to unique effects like superparamagnetism, enhanced magnetization and (below a critical dimension) single domain magnetic nanoparticles. Such nanoparticles exhibit single domain ferromagnetism below the blocking temperature, T_B, and superparamagnetism above T_B. In the superparamagnetic state, the moment of each nanoparticle freely rotates, so a collection of nanoparticles acts like a paramagnet where the constituent moments are ferromagnetic nanoparticles (rather than atomic moments as in a normal paramagnet). In the ZFC measurement of the magnetization as a function of temperature, the above behaviour leads to the presence of a peak at a temperature commonly taken as the blocking temperature. The features of the peak that reveals the superparamagnetic state (namely its width and position) and the behaviour of the high-temperature tail contain useful information about various characteristics of nanoparticles for example size and size distribution. While such information can be obtained accurately with the assumption of non-interacting magnetic nanoparticles, even simple comparison of curves of different nanoparticles is very useful since it can reveal how the nanoparticles evolve under an external control parameter like doping, annealing, etc.

As it is well known, above T_B, superparamagnetic moment of particles becomes thermally unstable and

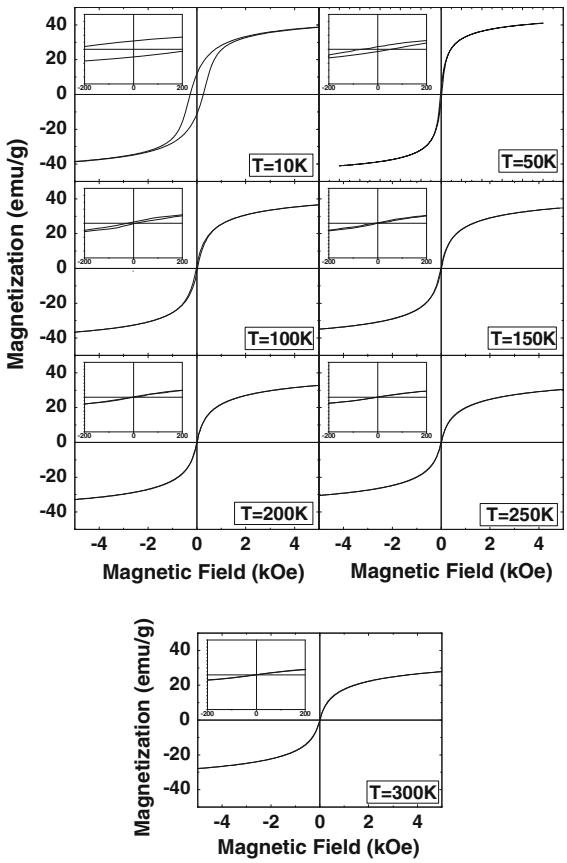

Fig. 5 M–H loops of $Mn_{0.2}Ni_{0.8}Fe_2O_4$ NP's at some selected temperatures. *Insets* show the zoomed part of M–H curves for the corresponding temperatures with a magnetic field scale of ±200 Oe

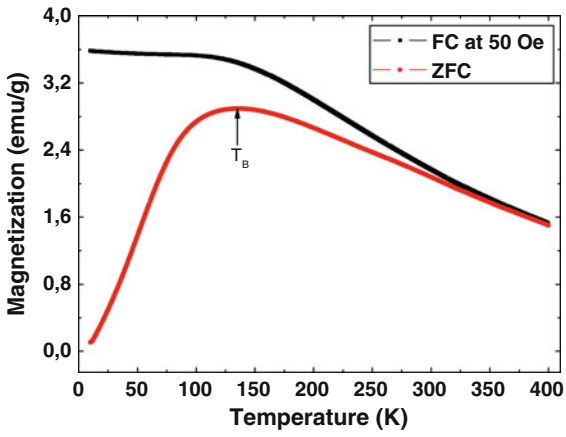

Fig. 6 Temperature variation of magnetization of $Mn_{0.2}Ni_{0.8}Fe_2O_4$ NPs with 50 Oe applied field

magnetizations exponentially decrease as MVH/k_BT become smaller than 1. The superparamagnetic particles deflect uniquely to the strong field side of the gradient magnet, but this effect decreases as a function of increasing temperature. Above the blocking temperature T_B, the thermal fluctuation energy (k_BT) is larger than the uniaxial anisotropy energy (KV), because the critical volume for nanoparticles behaving as a single domain is larger than the studied magnetic particles (Pelecky and Rieke 1996; Köseoglu and Kavas 2008; Özkaya et al. 2009). At high temperature regime, assuming an equilibrium state, the magnetic susceptibility follows a Curie–Weiss law (Sawatsky et al. 1968) with a ferromagnetic transition temperature T_c. H_c and M_r have shown superparamagnetic behaviours by increasing the temperature above the blocking temperature. Below the blocking temperature, T_B, the uniaxial anisotropy energy (KV) is larger than the thermal fluctuation energy (k_BT) and the magnetic moments of the particles are magnetically frozen along their anisotropy axes.

Consequently, the magnetization of the nanoparticles has a hysteretic feature. The decrease in magnetization below T_B should be attributed to this spin frustration in spin-glass like phase. A spin-glass-like ordering of magnetic moments may be thought of for the random distribution of magnetic dipoles. This is consistent with spin-canting due to the decrease in effective super exchange interactions among magnetic spins at the surface regions, which reflects itself as a decrease of average magnetization of single particle domain as mentioned above.

ac/dc conductivity

Figure 7 shows *ac* electrical conductivity, σ_{ac}, of $Mn_{0.2}Ni_{0.8}Fe_2O_4$ nanoparticles as a function frequency at some selected temperatures. From the plot, it is evident that the electrical conductivity is stricktly frequency and temperature dependent. The σ_{ac} slightly changes between 1 Hz–1 kHz at all temperatures.Above this frequency, it increases fast. Also, by increasing the temperature, the σ_{ac} increases sharply as it can be seen from figure.

Figure 8 shows the temperature dependence of dc conductivity, σ_{dc}, of the sample which was derived from the plateau regions. As expected for semiconductors,

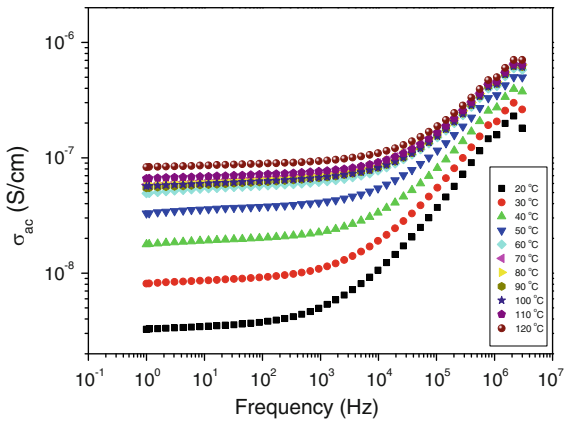

Fig. 7 Frequency dependence of ac conductivity at some selected temperatures

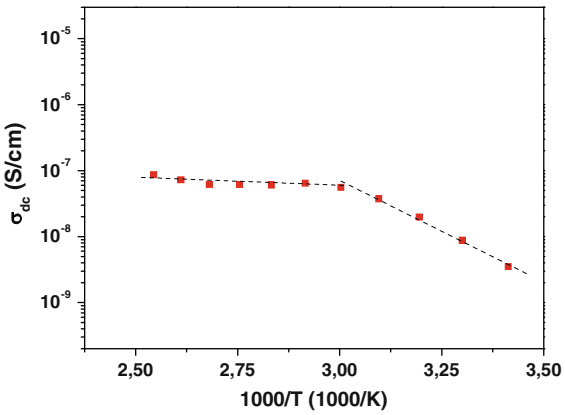

Fig. 8 Temperature dependent dc conductivity

the conductivity of ferrites increases with rising temperature according to the well-known relation

$$\sigma = \sigma_0 \exp(-E_a/kT) \quad (1)$$

where E_a denotes the thermal activation energy of electrical conduction, σ_o is pre-exponential parameter which depends on the semiconductor nature, and k is the Boltzmann's constant. As seen from dc conductivity graph, the conductivity of the sample is increasing with the temperature indicating the semiconducting nature of the sample. The increasing trend in the dc conductivity, σ_{dc}, with the temperature is due to the increase in drift mobility of the thermally activated charge carriers (electron and hole) according to hopping conduction mechanism.

The temperature dependence of σ_{dc} shows a straight line with two different activation energies. The line changes its slope at the Curie temperature T_c $\sim$360 K, as was expected theoretically (Kapse et al. 2009). It was reported that on passing through the Curie point a change in the gradient of the straight line (Fig. 8) must take place. The magnitude of this effect (gradient or slope) depends on the exchange interaction, which determines the Curie point, T_c (Sertkol et al. 2009).

Dielectric properties

The dielectric properties of NP ferrite materials are influenced mainly by the method of preparation, cation distribution, grain size, sintering temperature, oxygen parameter, the ratio of Fe^{2+}/Fe^{3+} ions, and oxygen anion vacancies in lattices out of which the grain size plays a key role (Mohammed et al. 2002).

The samples which assumed heterogeneous nature due to the individual grains influences the dielectric variation with frequency. Thus, the dielectric behaviour of the ferrites is attributed primarily to interfacial polarisation resulting from their heterogeneous structure comprising low resistivity grains separated by high resistivity grain boundaries as suggested by Koops phenomenological dispersion theory (Koops 1951; Miroshkin et al. 1981; Viswanathan and Murthy 1990). The Fe^{2+} and Fe^{3+} ions present in ferrites contribute effectively to produce interfacial polarisation. This is supported by the inverse proportionality between dielectric permittivity and resistivity as observed by various researchers.

The complex dielectric permittivity is represented $\varepsilon^* = \varepsilon' - i\varepsilon''$ where ε' is the real part of dielectric permittivity, which describes the stored energy, while ε'' is the imaginary part of dielectric permittivity, which describes the dissipated energy (Farea et al. 2008). The frequency and temperature dependence effects on both ε' and ε'' are shown in Fig. 9.

It is clear that the sample exhibits dielectric dispersion where both ε' and $\varepsilon''$of the studied system show a decrease with increasing frequency. The values of ε'' decreases faster than ε' and becomes closer in the high-frequency range. The decrease in dielectric constant is rapid at low frequency and approach to frequency independent behaviour. The dielectric dispersion curve can be explained on the basis of Koop's theory, which based on the Maxwell–Wagner model

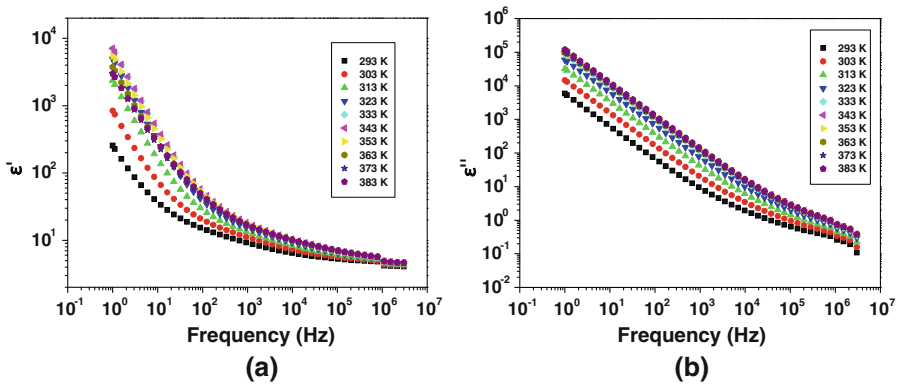

Fig. 9 Plots of real **a** ε' and imaginary, **b** $\varepsilon''$of dielectric constant versus frequency at some selected temperatures

for the homogeneous double structure (Farea et al. 2008). The polarization in ferrites is through a mechanism similar to the conduction process by electron exchange between Fe^{2+} and Fe^{3+}, the local displacement of electrons in the direction of the applied field occurs and these electrons determine the polarization. The polarization decreases by increasing the frequency and approaches to a constant value due to the electron exchange between Fe^{2+} and Fe^{3+} cannot follow the alternating field. Previously, the large value of dielectric constant at lower frequency was attrributed to the predominance of species like Fe^{2+} ions, oxygen vacancies, grain boundary defects, etc. (Maxwell 1973). The decrease in dielectric constant with frequency is expected because of the fact that any species contributing to polarizability is found to show lagging behind the applied field at higher and higher frequencies (Gul et al. 2007).

Figure 9 clearly shows the enhancement of dielectric permittivity at low frequencies. However, dielectric permittivity decreases at higher frequencies since the mobility of charge carriers is low at higher frequencies and cannot follow the alternation of applied ac electric field (Abdeen 1999). There are two mechanisms responsible for the permittivity dispersion for polycrystalline ferrites at higher frequency; they are ion and electron polarization (Psarras 2006). The oxygen ion vacancies produced during the synthesis may also contribute to dielectric permittivity which is predominant at lower frequencies (Ponpandian and Narayanasamy 2002).

It can be seen that the sample shows the frequency-dependent phenomena, i.e., the dielectric constant decreases with increasing frequency. This is a normal behaviour observed in most of the ferrimagnetic materials, which may be due to the interfacial polarization as predicted by Maxwell–Wagner (Wagner 1914). According to Rabinkin and Novikova (1960), the polarization in ferrites is through a mechanism similar to the conduction process. By electron exchange between Fe^{2+} and Fe^{3+}, the local displacement of electrons in the direction of the applied field occurs and these electrons determine the polarization. The polarization decreases with increasing frequency and then reaches a constant value due to the fact that beyond a certain frequency of external field, the electron exchange between Fe^{2+} and Fe^{3+} cannot follow the alternating field. The large value of ε'' at lower frequency is due to the predominance of species like Fe^{2+} ions, interfacial dislocations pile ups, oxygen vacancies, grain boundary defects, etc. (Maxwell 1973), while the decrease in ε'' with frequency is natural because of the fact that any species contributing to polarizability is found to show lagging behind the applied field at higher and higher frequencies.

Conclusion

In this study, manganese-substituted nickel ferrite nanoparticles of $Mn_{0.2}Ni_{0.8}Fe_2O_4$ have been prepared successfully by using surfactant-assisted hydrothermal route. Crystallite size of the product was found as 6 nm by using line profile fitting of XRD pattern. From magnetic measurements the absence of saturation, remanent magnetization and coercivity at high temperature region in the M–H curve and broad peak in ZFC indicates the superparamagnetic nature of the particles with a blocking temperature T_B of 130 K. The saturation magnetization of the sample increases with the decrease in temperature. It is observed that the dc

conductivity increases with increasing temperature indicating the semiconducting nature of the sample. This was attributed to the increase in drift mobility of the charge carriers. While the dielectric constant was found to decrease with frequency, it was increasing with the temperature as observed in semiconductors. Also, revealed sharply reduced dielectric loss in this nanomagnetic sample making it as a suitable candidate for applications as inductive and capacitive materials as well as microwave absorbers.

Acknowledgements This work is supported by Fatih University under BAP grant no. P50010701 and P50020902-2.

References

Abdeen AM (1999) Dielectric behaviour in Ni–Zn ferrites. J Magn Magn Mater 192:121–129. doi:10.1016/S0304-8853(98)00324-2

Anantharaman MR, Sindhu S, Jagatheesan S, Malini KA, Kurian P (1999) Dielectric properties of rubber ferrite composites containing mixed ferrites. J Physics D: Appl Phys 32:1801

Atif M, Hasanain SK, Nadeem M (2006) Magnetization of sol–gel prepared zinc ferrite nanoparticles: Effects of inversion and particle size. Solid State Commun 138:416–421. doi:10.1016/j.ssc.2006.03.023

Balaji G, Gajbhiye NS, Wilde G, Weissmüller J (2002) Magnetic properties of $MnFe_2O_4$ nanoparticles. J Magn Magn Mater 242–245:617–620. doi:10.1016/S0304-8853(01)01043-5

Chinnasamy CN, Narayanasamy A, Ponpandian N, Chattopadhyay K, Guerault H, Greneche J-M (2000) Magnetic properties of nanostructured ferrimagnetic zinc ferrite. J Phys 12:7795–7806. doi:10.1088/0953-8984/12/35/314

Farea AMM, Kumar S, Batoo KM, Yousef A, Lee CG, Alimuddin (2008) Structure and electrical properties of $Co_{0.5}Cd_xFe_{2.5-x}O_4$ ferrites. J Alloys Compd 464:361–369. doi:10.1016/j.jallcom.2007.09.126

Ghasemi A, Hossienpour A, Morisako A, Saakhi A, Saleki M (2006) Electromagnetic properties and microwave absorbing characteristics of doped barium hexaferrite. J Magn Magn Mater 302:429–435. doi:10.1016/j.jmmm.2005.10.006

Gul IH, Abbasi AZ, Amin F, Anis-ur-Rehman M, Maqsood A (2007) Structural, magnetic and electrical properties of $Co_{1-x}Zn_xFe_2O_4$ synthesized by co-precipitation method. J Magn Magn Mater 311:494–499. doi:10.1016/j.jmmm.2006.08.005

Kapse VD, Ghosh SA, Raghuwanshi FC, Kapse SD, Khandekar US (2009) Nanocrystalline $Ni_{0.6}Zn_{0.4}Fe_2O_4$: a novel semiconducting material for ethanol detection. Talanta 78:19–25. doi:10.1016/j.talanta.2008.10.031

Kasapoglu N, Baykal A, Köseoğlu Y, Toprak MS (2007) Microwave-assisted combustion synthesis of $CoFe_2O_4$ with urea, and its magnetic characterization. Scripta Mater 57:441–444. doi:10.1016/j.scriptamat.2007.04.042

Kavas H, Baykal A, Toprak MS, Köseoğlu Y, Sertkol M, Aktas B (2009) Cation distribution and magnetic properties of Zn doped $NiFe_2O_4$ nanoparticles synthesized by PEG-assisted hydrothermal route. J Alloys Compd 479:49–55. doi:10.1016/j.jallcom.2009.01.014

Koops CG (1951) On the dispersion of resistivity and dielectric constant of some semiconductors at audiofrequencies. Phys Rev 83:121–124. doi:10.1103/PhysRev.83.121

Köseoğlu Y, Kavas H (2008) Size and surface effects on magnetic properties of Fe_3O_4 nanoparticles. J Nanosci Nanotechnol 8:584–590. doi:10.1166/jnn.2008.B012

Kuznetsov MV, Barquın LF, Pankhurst QA, Parkin IV (1999) Self-propagating high-temperature synthesis of barium-chromium ferrites $BaFe_{12-x}Cr_xO_{19}$ (0 *x*6.0). J Phys D 32:2590–2598. doi:10.1088/0022-3727/32/20/302

Li F, Wang H, Wang L, Wang J (2007) Magnetic properties of $ZnFe_2O_4$ nanoparticles produced by a low-temperature solid-state reaction method. J Magn Magn Mater 309:295–299. doi:10.1016/j.jmmm.2006.07.012

Liu J, Xua T, Gong M, Yu F (2006) Fundamental studies of novel inorganic–organic charged zwitterionic hybrids: 4. New hybrid zwitterionic membranes prepared from polyethylene glycol (PEG) and silane coupling agent. J Membr Sci 283:190–200. doi:10.1016/j.memsci.2006.06.027

Maxwell JC (1973) Electricity and magnetism. Oxford University Press, NewYork, p 828

McMichael RD, Shull RD, Swartzendruber IJ, Bennett LH (1992) Magnetocaloric effect in superparamagnets. J Magn Magn Mater 111:29–33. doi:10.1016/0304-8853(92)91049-Y

Miroshkin VP, Panova YAI, Passynkov VV (1981) Dielectric relaxation in polycrystalline ferrites. Phys Stat Sol A 66:779–782. doi:10.1002/pssa.2210660245

Mohammed EM, Malini KA, Kurian P, Anantharaman MR (2002) Modification of dielectric and mechanical properties of rubber ferrite composites containing manganese zinc ferrite. Mater Res Bull 37:753–768. doi:10.1016/S0025-5408(02)00690-6

Ozkaya T, Baykal A, Toprak MS, Köseoğlu Y, Durmus Z (2009) Reflux synthesis of Co_3O_4 nanoparticles and its magnetic characterization. J Magn Magn Mater 321:2145–2149. doi:10.1016/j.jmmm.2009.01.003

Özkaya T, Toprak MS, Baykal A, Kavas H, Köseoğlu Y, Aktaş Synthesis B (2009) Synthesis of Fe_3O_4 nanoparticles at 100 °C and its magnetic characterization. J Alloys Compd 472:18–23. doi:10.1016/j.jallcom.2008.04.101

Pelecky DL, Rieke RD (1996) Magnetic properties of nanostructured materials. Chem Mater 8:1770–1783. doi:10.1021/cm960077f

Pielaszek R (2003) Analytical expression for diffraction line profile for polydispersive powders. Appl crystallogr. In: Proceedings of the XIX Conference, Krakow, Poland, pp 43–50

Ponpandian N, Narayanasamy A (2002) Influence of grain size and structural changes on the electrical properties of nanocrystalline zinc ferrite. J Appl Phys 92(5):2770–2778. doi:10.1063/1.1498883

Psarras GC (2006) Hopping conductivity in polymer matrix–metal particles composites. Compos A 37:1545–1553. doi:10.1016/j.compositesa.2005.11.004

Rabinkin LI, Novikova ZI (1960) Ferrites. Minsk, p 146

Ravinder D, Reddy AVR, Rangamohan G (2002) Abnormal dielectric behaviour in polycrystalline zinc-substituted manganese ferrites at high frequencies. Mater Lett 52:259–265. doi:10.1016/S0167-577X(01)00404-9

Reddy SV, Radhe Shyam A, Dwivedi R, Gupta RK, Chumbale VR, Prasad R (2004) *Ortho*-selective vapour phase methylation of phenol over nanocrystalline ferrospinels of varying Zn^{2+}/Mn^{2+} ionic composition. J Chem Technol Biotechnol 79:1057–1064. doi:10.1002/jctb.1060

Rondinone AJ, Samia ACS, Zhang ZJ (1999) Superparamagnetic relaxation and magnetic anisotropy energy distribution in $CoFe_2O_4$ spinel ferrite nanocrystallites. J Phys Chem B 103:6876–6880. doi:10.1021/jp9912307

Sahoo Y, Cheon M, Wang S, Luo H, Furlani EP, Prasad PN (2004) Field-directed self-assembly of magnetic nanoparticles. J Phys Chem B 108:3380–3383. doi:10.1021/jp031148i

Sawatsky A, van der Woude F, Morrish AH (1968) Cation distributions in octahedral and tetrahedral sites of the ferrimagnetic spinel $CoFe_2O_4$. J Appl Phys 39:1204–1206. doi:10.1063/1.1656224

Sertkol M (2008) Synthesis and magnetic characterization of microwave absorbing materials. Master Thesis, Fatih University, Istanbul

Sertkol M, Köseoğlu Y, Baykal A, Kavas H, Basaran AC (2009a) Synthesis and magnetic characterization of $Zn_{0.6}Ni_{0.4}Fe_2O_4$ nanoparticles via a polyethylene glycol-assisted hydrothermal route. J Magn Magn Mater 321:157–162. doi:10.1016/j.jmmm.2008.08.083

Sertkol M, Köseoğlu Y, Baykal A, Kavas H, Bozkurt A, Toprak MS (2009b) Microwave synthesis and characterization of Zn-doped nickel ferrite nanoparticles. J Alloys Compd 486:325–329. doi:10.1016/j.jallcom.2009.06.128

Sertkol M, Köseoğlu Y, Baykal A, Kavas H, Toprak MS (2010) Synthesis and magnetic characterization of $Zn_{0.7}Ni_{0.3}Fe_2O_4$ nanoparticles via microwave-assisted combustion route. J Magn Magn Mater 322:866–871. doi:10.1016/j.jmmm.2009.11.018

Shyam AR, Dwivedi R, Reddy VS, Chary KVR, Prasad R (2002) Vapour phase methylation of pyridine with methanol over the $Zn_{1-x}Mn_xFe_2O_4$ ($x = 0$, 0.25, 0.50, 0.75 and 1) ferrite system. Green Chem 4:558–561. doi:10.1039/b207410a

Smith J, Wijn HPJ (1959) Ferrites: physical properties of ferromagnetic oxides in relation to their technical applications. Wiley, New York

Upadhyay C, Verma HC, Sathe V, Pimpale AV (2007) Effect of size and synthesis route on the magnetic properties of chemically prepared nanosize $ZnFe_2O_4$. J Magn Magn Mater 312:271–279. doi:10.1016/j.jmmm.2006.10.448

Viswanathan B, Murthy VRK (1990) Ferrite materials: science and technology. Springer-Verlag, Berlin and Heidelberg, GmbH & Co. KG

Wagner KW (1914) Arch Elektrotechn 2:371

Wejrzanowski T, Pielaszek R, Opalińska A, Matysiak H, Lojkowski W, Kurzydlowski KJ (2006) Quantitative methods for nanopowders characterization. Appl Surf Sci 253:204–208. doi:10.1016/j.apsusc.2006.05.089

Xiaotun Y, Lingge X, Choon NS, Hardy CS (2003) Magnetic and electrical properties of polypyrrole-coated γ-Fe_2O_3 nanocomposite particles. Nanotechnology 14:624–629. doi:10.1088/0957-4484/14/6/311

Zhang ZJ, Chen XY, Wang BN, Shi CW (2008) Hydrothermal synthesis and self-assembly of magnetite (Fe_3O_4) nanoparticles with the magnetic and electrochemical properties. J Cryst Growth 310:5453–5457. doi:10.1016/j.jcrysgro.2008.08.064

Zhou B, Zhang YW, Liao CS, Yan CH (2002) Magnetism and phase transition for $CoFe_{2-x}Mn_xO_4$ nanocrystalline thin films and powders. J Magn Magn Mater 247:70–76. doi:10.1016/S0304-8853(02)00150-6

Zhou L, Cui Y, Hua Y, Yu L, Jin W, Feng S (2006) The magnetic properties of $Ni_{0.7}Mn_{0.3}Gd_xFe_{2-x}O_4$ ferrite. Mater Lett 60:104–108. doi:10.1016/j.matlet.2005.07.083